Origin of Slow Cortical Oscillations in Deafferented Cortical Slabs

I. Timofeev, F. Grenier, M. Bazhenov[1], T.J. Sejnowski[1,2] and M. Steriade

Laboratory of Neurophysiology, School of Medicine, Laval University, Quebec, Canada G1K 7P4, [1]Howard Hughes Medical Institute, The Salk Institute, Computational Neurobiology Laboratory, 10010 North Torrey Pines Road, La Jolla, CA 92037 and [2]Department of Biology, University of California, La Jolla, CA 92093, USA

An *in vivo* preparation has been developed to study the mechanisms underlying spontaneous sleep oscillations. Dual and triple simultaneous intracellular recordings were made from neurons in small isolated cortical slabs (10 mm × 6 mm) in anesthetized cats. Spontaneously occurring slow sleep oscillations, present in the adjacent intact cortex, were absent in small slabs. However, the isolated slabs displayed brief active periods separated by long periods of silence, up to 60 s in duration. During these silent periods, 60% of neurons showed non-linear amplification of low-amplitude depolarizing activity. Nearly 40% of the cells, twice as many as in intact cortex, were classified as intrinsically bursting. In cortical network models based on Hodgkin–Huxley-like neurons, the summation of simulated spontaneous miniature excitatory postsynaptic potentials was sufficient to activate a persistent sodium current, initiating action potentials in single neurons that then spread through the network. Consistent with this model, enlarging the isolated cortical territory to an isolated gyrus (30 mm × 20 mm) increased the probability of initiating large-scale activity. In these larger territories, both the frequency and regularity of the slow oscillation approached that generated in intact cortex. The frequency of active periods in an analytical model of the cortical network accurately predicted the scaling observed in simulations and from recordings in cortical slabs of increasing size.

Introduction

The reduction of neural elements to a minimal number, as in brain slices and tissue cultures, is often used to investigate elementary properties of more complex systems. In these simplified preparations, cortical neurons display relatively stereotyped intrinsic electrophysiological properties and the network is generally silent, with the exception of miniature synaptic events, termed minis (Redman, 1990; Salin and Prince, 1996). In earlier studies, the isolated cortical slabs *in vivo* had no spontaneous activity (Burns, 1950) or displayed paroxysmal, epileptic-like discharges (Echlin *et al.*, 1952). Electrical stimulation in cortical slices usually elicits excitatory and inhibitory postsynaptic potentials (EPSPs and IPSPs), while network synchronized activity may be observed with certain compositions of the bath solution and propagation of excitation occurs in slightly disinhibited slices (Avoli, 1986; Connors *et al.*, 1988; Chagnac-Amitai and Connors, 1989). In contrast, the intact cerebral cortex exhibits *in vivo* a rich repertoire of spontaneously occurring low-frequency (Steriade *et al.*, 1993b,c; Achermann and Borbély, 1997) and high-frequency oscillations (Llinás and Ribary, 1993; Steriade *et al.*, 1993b; Gray and McCormick, 1996; Steriade *et al.*, 1996) that may alter the expression of firing patterns produced by intrinsic neuronal properties (Steriade *et al.*, 1998a), and cortical responses to afferent volleys are followed by self-sustained rhythmic activities (Steriade *et al.*, 1998b).

A key question in an interconnected system is whether increasing its size and connectivity can lead to new properties (Watts and Strogatz, 1998). What causes the presence of spontaneously synchronized activity in the intact cortex, compared to the absence of such activity in slice preparations? Two main factors could explain this difference. The first is the number of interconnected neurons. Even a small increase in the thickness of a cortical slice from 0.4 to 0.5 mm results in a 4- to 5-fold increase in connectivity between pyramidal and non-pyramidal neurons (Thomson *et al.*, 1996). Secondly, the intrinsic properties of cortical neurons and response patterns remain similar over long-term recordings in constant *in vitro* conditions (Schwindt *et al.*, 1997; Gupta *et al.*, 2000), but they are expressed differently with increased synaptic activity (Steriade, 1997; Steriade *et al.*, 1998a) and with changes in the membrane potential (V_m) due to the presence of modulatory systems *in vivo* (Steriade *et al.*, 1993a) or application of activating neurotransmitters *in vitro* (Wang and McCormick, 1993).

To examine the issue of scaling the size of the network without drastically changing the milieu of the neurons in the network, we developed a new preparation that has advantages of both the *in vitro* and *in vivo* preparations. Experimental recordings from small cortical slabs isolated from thalamic and cortical inputs, as well as from a larger isolated gyrus, revealed that activity was sparse and irregular in smaller slabs, but became progressively more similar to the slow oscillations observed in the intact cortical tissue as the size of the slab was increased. In computational models of the cortical network that closely matched the experimental recordings, the initiation event occurred in single cortical neurons driven by spontaneous miniature excitatory postsynaptic activity and spread by recruiting neighboring neurons. Thus, the variability expressed in large-scale activity during sleep states *in vivo* may reflect events that are initiated in single neurons.

Material and Methods

Experimental Design

Experiments were carried out on 35 adult cats anesthetized with ketamine and xylazine (10–15 and 2–3 mg/kg). Under this type of anesthesia, the electrographic pattern consists of a slow oscillation at <1 Hz, mainly 0.6–0.9 Hz (Steriade *et al.*, 1993c; Amzica and Steriade, 1995a; Contreras and Steriade, 1995), very similar to that of the slow oscillation during natural sleep in cats (Steriade *et al.*, 1996) and humans (Achermann and Borbély, 1997; Amzica and Steriade, 1997). The EEG was monitored continuously during the experiments to maintain a deep level of anesthesia and additional doses of anesthetic were given at the slightest tendency toward an activated EEG pattern. In addition, all pressure points and tissues to be incised were infiltrated with lidocaine. The cats were paralyzed with gallamine triethiodide and artificially ventilated to an end-tidal CO_2 of 3.5–3.8%. The heartbeat was monitored and kept constant (90–110 beats/min). Body temperature was maintained at 37–39°C. Glucose saline (5% glucose, 10 ml i.p.) was given every 3–4 h during experiments, which lasted for 8–14 h.

Isolated slabs (Fig. 1) were prepared from areas 5 and 7 of the

suprasylvian gyrus in 29 cats. After opening a hole in the parietal bone, a small perforation was made in the dura above a part of the pia that did not contain large vessels. A custom crescent knife was inserted along its curve into the cortex until the tip of the knife appeared ~10 mm frontally under the pia. The knife was then turned by 90° in both right and left directions. The pia was intact except at the place the knife was entered. Such slabs were ~8–10 mm long (rostro-caudal direction), ~5–6 mm wide (medio-lateral direction) and ~4–5 mm deep (Fig. 1*a*,*b*). Slabs showing signs of edema and/or bleeding were not recorded. The completeness of neuronal transections and the boundaries of the slab were verified in every case on 80 μm thionine-stained sections (Fig. 1*b*). In six other cats, we isolated the suprasylvian gyrus (Fig. 1*c*) by making longitudinal cuts through marginal and ectosylvian gyri. Thereafter, by using an oblique approach we inserted a spatula and undercut the white matter 7–8 mm below the surface of the suprasylvian gyrus. The size of the isolated gyrus was 30 mm × 20 mm.

Field potential recordings were obtained and stimulation delivered by means of bipolar coaxial macroelectrodes inserted in the slab as well as outside the slab (adjacent suprasylvian areas and/or precruciate area 4) for control EEG recordings. The outer pole of the electrode was placed at the cortical surface or 0.1 mm deeper and the inner pole was placed at 0.8–1 mm of cortical depth. The micropipettes for intracellular recordings in the cortex were placed in the vicinity of at least one EEG electrode. Sharp glass micropipettes were filled with a solution of 2.5–3 M potassium acetate (DC resistance of 30–80 MΩ. In some experiments, QX-314 (50 mM) was added to the pipette solution. A high-impedance amplifier (bandpass 0–10 kHz) with active bridge circuitry was used to record and inject current into the cell. The signals were recorded on an eight-channel tape with bandpass of 0–9 kHz and digitized at 10–20 kHz for offline computer analysis. The stability of intracellular recordings was ensured by cisternal drainage, bilateral pneumothorax, hip suspension and by filling the hole made in the skull with a solution of agar-agar (4%). At the end of all experiments the cats were given a lethal dose of pentobarbitone and perfused intracardially with physiological saline followed by 4% formaldehyde and 1% glutaraldehyde.

Neuron and Network Models

Each cortical neuron was modeled by two compartments coupled by a 10 MΩ resistance. The ionic currents in the model were taken from a previous study (Mainen and Sejnowski, 1996), with the addition of a persistent sodium current, $I_{Na(p)}$ (Alzheimer *et al.*, 1993; Kay *et al.*, 1998) (See Appendix for details). The firing pattern of the compartmental model neuron was controlled by the parameter ρ, which is the ratio of the surface area of the dendritic compartment to the somatic compartment. For the cortical pyramidal (PY) cells, ρ = 165 to match the intrinsically bursting responses observed in the majority of pyramidal cells in the slab (Fig. 2) and ρ = 50 for interneuron (IN) to obtain regular firing patterns. The addition of a $I_{Na(p)}$ to the model increased the bursting of the PY cells compared to the original model (Mainen and Sejnowski, 1996). In some simulations we varied ρ around the average value randomly by 10–20% to test the effects of variability on the firing patterns of PY and IN cells. Some of the intrinsic parameters (such as the maximal conductances for the $I_{Na(p)}$, the high-threshold Ca^{2+} current and the fast voltage-dependent sodium and potassium currents and resting membrane potentials of the neurons) were initialized around the mean with a random variability of ~10% to ensure robust results. In most of the simulations the synaptic conductances were 0.11 μS for AMPA between PY cells, 0.05 μS for AMPA from PY to IN, and 0.05 μS for $GABA_A$ from IN to PY. In some simulations these parameters were varied, as indicated, which affected slightly the duration of active patterns and interburst intervals. The expressions for voltage- and Ca^{2+}-dependent transition rates for all currents are given in the Appendix.

The cortical model consisted of a one-dimensional two-layer array of N PY and N IN cells with local connectivity, where N was varied from 50 to 2000. More inhibitory neurons were included (50% of total population) than found in cortex (~20%) but the maximal conductance of the inhibitory synapses was diminished. This reduced the synchronizing effects of the interneurons, which were enhanced in our model due to the limited number of synapses per cell. In the smaller networks (smaller N), if we reduce a relative number of IN cells but keep the total $GABA_A$ conductance per cell constant, the size of individual IPSPs becomes enormously large so IN spikes effectively synchronized all their post-synaptic PY cells and also terminated active patterns very quickly. Thus, in our model we did not specifically model the columnar organization with a proper ratio of PY and IN cells but instead approximated each cortical column by single PY–IN pair. In all models, each PY cell made AMPA-mediated connections with all other cells within a fixed radius of four cells, which included eight PY cells and nine IN cells, and each IN cell made $GABA_A$-mediated connections with PY cells within the same radius. A simple model was used to describe short-term depression of excitatory and inhibitory synaptic connections (Tsodyks and Markram, 1997; Galarreta and Hestrin, 1998). All AMPA and $GABA_A$ synapses were modeled by first-order activation schemes and the kinetic model and parameter values are given in the Appendix (Bazhenov *et al.*, 1998). Figure 2*a* shows a typical bursting pattern of a cortical neruon in response to current injection and Figure 2*d* shows temporal summation of EPSPs following a burst of action potentials in a presynaptic neuron.

Spontaneous miniature EPSPs and miniature IPSPs followed the same equations as the regular PSPs and their arrival times were modeled by Poisson processes (Stevens, 1993), with time-dependent mean rate $\mu(t)$ (see below).

Analytical Model

The analytical model for the distribution of interburst intervals is based on the probability of a burst occurring in a single neuron as a function of time since the last burst. Assume that n miniature EPSPs need to occur in a time window δt to depolarize the membrane sufficiently to activate the $I_{Na(p)}$. Although this assumption is a simplification, it permits the probability distribution function to be calculated analytically with good accuracy. For a Poisson-distributed train of miniature EPSPs the probability to activate the persistent sodium current, and generate a new burst at time instant $k\delta t$ after the last one is

$$\begin{aligned} P(k) &= \prod_{s=0}^{k-1} P_{<n}(s)\left[1-P_{<n}(k)\right] \\ P_{<n}(s) &= e^{-\mu(s)M}\left\{1+\mu(s)\delta tM+\cdots+\frac{\left[\mu(s)\delta tM\right]^{n-1}}{(n-1)!}\right\} \end{aligned} \tag{1}$$

where n is critical number of miniature EPSPs that have to occur inside the time window δt to bring a pyramidal cell to the threshold, $P_{<n}(s)$ is the probability of finding less than n miniature events at the time interval $[s\delta t,(s+1)\delta t]$, M is the total number of synapses for one cells, $\mu(s)$ is the mean rate of Poisson processes. If $f = \mu(s)\delta t\, M << 1$, then

$$\begin{aligned} P(k) &\approx P_{>n}(k)\exp\left[-\sum_{s=0}^{k-1} P_{>n}(s)\right] \\ P_{>n}(k) &= 1-P_{<n}(k) \approx e^{-f}\frac{f^n}{n!} \end{aligned} \tag{2}$$

where $P_{>n}(s)$ is the probability of finding n or more miniature events at the interval $[s\delta t,(s+1)\delta t]$. For a network with N pyramidal cells:

$$P_N(k) \approx N\exp\left[-(N-1)\sum_{s=0}^{k} P_{>n}(s)\right]P(k) \tag{3}$$

The mean firing rate for the Hodgkin–Huxley model was approximated by either a logarithmic or sigmoid function:

$$\mu_1(s)=\frac{\log\left[(s\delta t+50)/50\right]}{400} \text{ or } \mu_2(s)=\frac{\left[2/\left(1+e^{-s\delta t/5000}\right)-1\right]}{40} \tag{4}$$

and the *in vivo* data as fit with the rate function:

$$\mu_3(s) = \frac{\left[2/\left(1+e^{-s\delta t/900}\right)-1\right]}{66} \quad (5)$$

Note that for the sigmoid distributions, the rate of minis approaches a constant value. Using the probability distribution function $P_N(k)$ above we calculated the mean period T between spontaneous bursting and its standard deviation σ:

$$T = \delta t \sum_{k=1}^{\infty} kP_N(k), \quad \sigma = \left[\sum_{k=1}^{\infty} (\delta tk - T)^2 P_N(k)\right]^{\frac{1}{2}} \quad (6)$$

Results

Resting Properties and Bursting Neurons in Isolated Cortical Slabs

Recordings were made from neocortical neurons in cats under ketamine–xylazine anesthesia. Spontaneous and evoked activities were recorded from small cortical slabs, from an isolated gyrus, and from neocortical areas that had intact connections. Isolated slabs (~10 mm × 6 mm) were prepared from association areas 5 and 7 of the suprasylvian gyrus (Fig. 1*a*,*b*). In other cats, we isolated the whole suprasylvian gyrus (~20 mm × 10 mm), which extends from the marginal to the ectosylvian gyri (Fig. 1*c*).

Data are based on single (n = 95), dual (n = 44) and triple (n = 9) simultaneous intracellular recordings, in conjunction with field potential, from superficial and deep cortical layers. Twenty-four neurons were recorded with QX-314-filled pipettes. The mean V_m of neurons in small cortical slabs was –70.4 ± 0.8 mV and the mean input resistance (R_{in}) was 48.6 ± 4.7 MΩ (range 30–120 MΩ). Compared to our database of >1000 neocortical neurons recorded from intact neocortical areas, showing a mean V_m of –62 mV and a mean R_{in} of 22 MΩ, the neurons in cortical slabs displayed a more negative V_m and a much higher R_{in}. The more negative V_m and large increase in R_{in} of neurons recorded from isolated cortical slabs, in which the spontaneous synaptic activity is greatly reduced compared to the intact cortex, corroborate recent experimental and modeling studies comparing the resting properties of neocortical pyramidal neurons during periods with intense synaptic activity *in vivo* with the properties of pyramidal neurons after microperfusion with TTX or *in vitro* (Paré *et al.*, 1998; Destexhe and Paré, 1999).

Another important difference was that, in slabs, intrinsically bursting (IB) neurons were twice as numerous as in intact cortical areas. These neurons have been described *in vitro* (Connors *et al.*, 1982; McCormick *et al.*, 1985) and *in vivo* (Nuñez *et al.*, 1993). In our database of *in vivo* neocortical cells, the proportion of IB neurons was 15–20%. In the present series of experiments conducted on isolated slabs, with a more hyperpolarized V_m of cortical neurons and decreased synaptic activity, the IB cells constituted 39% of all neurons (48 of 124). Figure 2*a* shows an example of an IB neuron recorded at rest. A depolarizing current pulse (0.5 nA, 0.2 s) resulted in the generation of three high-frequency spike-bursts. A slight DC depolarization of the same neuron converted the burst firing into a regular-spiking (RS) pattern. Similar changes, from IB to RS patterns, were obtained by synaptic activation of increasing strength. High-frequency (100 Hz) pulse-trains at slight intensities (0.12 mA) applied to cortex resulted in bursting responses of IB cells; however, an increased intensity of electrical stimuli (0.75 mA) invariably suppressed the bursting responses and revealed single action potentials (not shown).

What is the impact of spike-bursts, compared to single spikes, on synaptic transmission? The summated postsynaptic response elicited by a spike-burst should be greater than that elicited by a single spike. From single-axon EPSPs studies *in vitro*, it is known that the pyramid-to-pyramid connections mainly display paired-pulse depression, while pyramid-to-interneurons connections may display either paired-pulse facilitation or depression (Markram, 1997; Thomson, 1997; Thomson and Deuchars, 1997; Gupta *et al.*, 2000). The simultaneously recorded neurons from the *in vivo* slab (Fig. 2*b*) revealed an apparently direct connection from a presynaptic IB neuron to a postsynaptic RS neuron. This was seen in three neuronal pairs. Virtually every spike in the presynaptic neurons elicited a depolarizing response (failure rate 2%), with a latency of 1.2 ± 0.1 ms, measured from the top of the spike to the onset of the EPSP. Direct depolarization of the IB cell resulted in the generation of a high-frequency burst, followed by single-spike firing. In all cases (n = 105), the burst-evoked postsynaptic response in the RS neuron was greater in amplitude than the responses of the same neuron during the tonic firing mode in the presynaptic IB cell (Fig. 2*b*) as a result of sublinear temporal summation.

Spontaneous Activities in Isolated Cortical Small Slabs

Field potentials and intracellular recordings from small cortical slabs showed that the network was in a silent state most of the time. In 23 of 29 experiments with small slabs, the field potentials and intracellular recordings revealed the presence of periodic (2–6 min^{-1}) large amplitude depolarizing events (Fig. 3). Similar depolarizing events could be elicited by low-intensity electrical stimulation in all (n = 23) relatively 'active' slabs and in four out of six totally silent slabs (see below, Fig. 6). In the remaining two slabs, electrical stimulation within the slab resulted in short-lasting EPSP–IPSP sequences (up to 0.2 s), without self-sustained oscillations, similar to what usually occurs in the *in vitro* slice preparation.

The spontaneous depolarizing events originated from the baseline, lasted for 0.5–3 s (1.5 ± 0.1 s), were sometimes crowned by action potentials (0–32 spikes in different cells and different bursts; mean 4.3 ± 1.2 spikes per burst), and stood in clear contrast to the spontaneous slow oscillation in the intact cortex (Fig. 3*a*) (n = 19). Many more action potentials were recorded during the depolarizations from IB neurons (0–32 spikes, mean 16.0 ± 1.8) than from RS neurons (0–8 spikes, mean 3.1 ± 0.7). Examination of V_m fluctuations during the silent state of the network revealed the presence of small amplitude depolarizing potentials (SDPs), but action potentials were never observed between the bursts. Because all neurons from which stable, long-lasting recordings were obtained never displayed action potentials during the inter-burst lulls, the SDPs were most likely spike-independent minis, as described at the neuromuscular junction (Fatt and Katz, 1952) and also found in central structures, including the cerebral cortex (Redman, 1990; Paré *et al.*, 1997). The maximum of the first derivative of the voltage trace was used to select the SDPs. This method did not allow us to select all fluctuations of baseline and some of the very small amplitude or very slowly rising phase potentials were not included in the analysis. The averaged SDPs lasted from 15 to 40 ms, with a mode at 20 ms (Fig. 3*b*). The selected potentials from the same neuron varied in amplitude from 0.2 to 1.3 mV, with a mean amplitude of 0.54 ± 0.02 mV (Fig. 3*b*). The time distribution of these SDPs indicates that they occurred quite regularly (10–15 events/s), although no true rhythmicity was observed. The incidence of SDPs increased at the onset of field

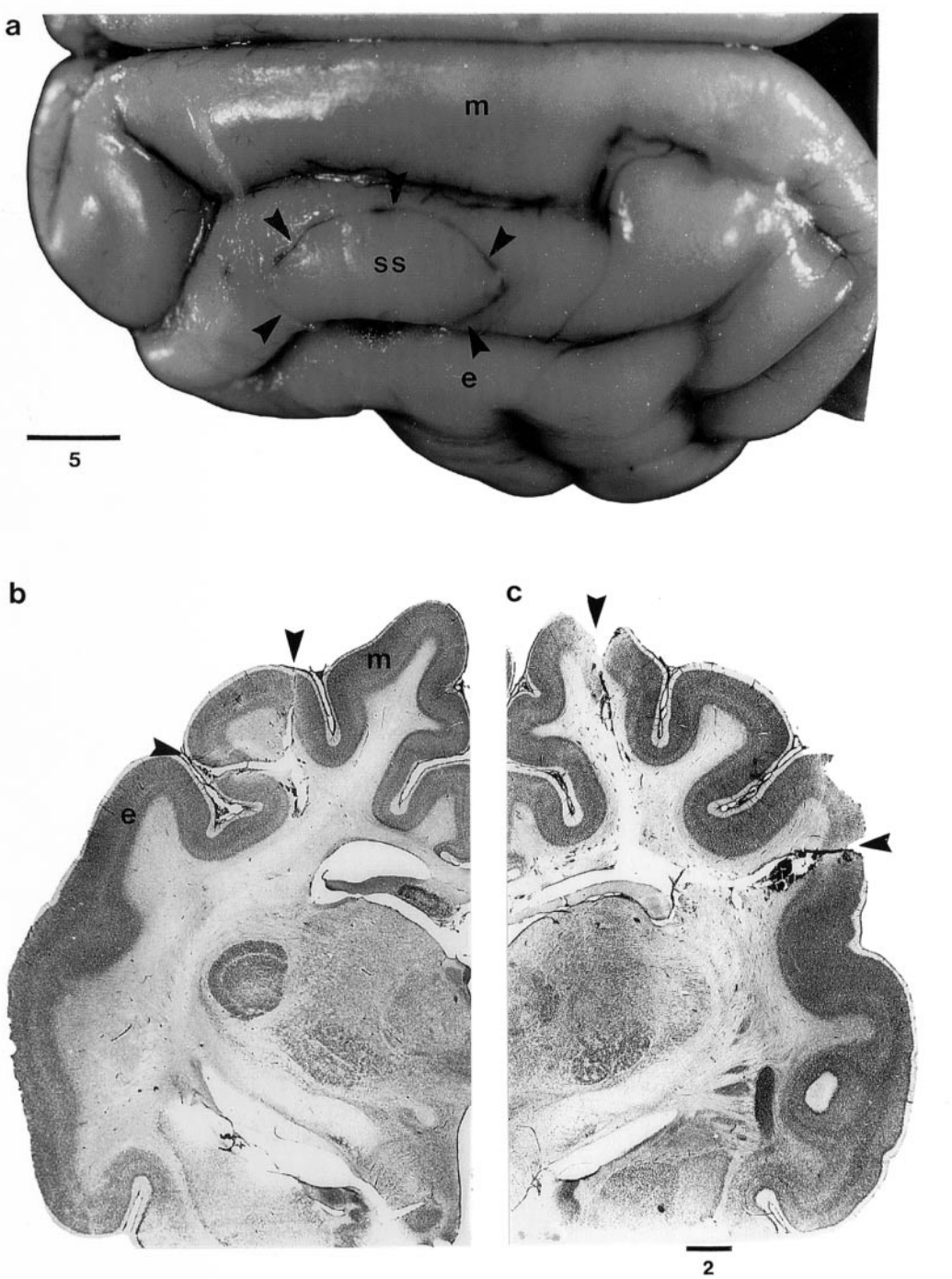

Figure 1. The neocortical slab *in vivo*. Slabs were prepared from areas 5 and 7 of the suprasylvian gyrus of ketamine-xylazine anesthetized cats. (*a*) Dorsal view of the left hemisphere. The limits of a slab within the suprasylvian (ss) gyrus are indicated by arrowheads. Other indicated gyri are marginal (m) and ectosylvian (e). (*b*) Frontal section in the left hemisphere showing a slab in the suprasylvian gyrus (between arrowheads). The pia mater was intact with the exception of the place where the knife entered. (*c*) Frontal section in the right hemisphere showing the isolated suprasylvian gyrus with parts of the adjacent marginal and ectosylvian gyri. Horizontal bars indicate mm.

and intracellular bursts of activity, which suggests that the sudden depolarizations observed in the slab could be triggered by summation of SDPs (Fig. 3*c*). After the burst cessation, the SDPs were significantly ($P < 0.05$, $n = 7$) suppressed for 1–2 s (Fig. 3*c*) and thereafter progressively recovered.

The SDPs in isolation could not depolarize neurons from the resting V_m, i.e. –70 mV, to a level sufficient for spike generation. To produce a significant depolarization, these small signals had to be summated and/or amplified. Several non-exclusive factors may account for such amplification. One of them may be represented by some intrinsic properties of neurons, which are usually masked by ongoing spontaneous activity in the intact-cortex preparations, and thus are only revealed during silent states. In fact, neurons recorded from slabs had a propensity to enhance small-amplitude depolarizing inputs (26 out of 32 tested neurons). Short (5 ms), subthreshold current pulses elicited an

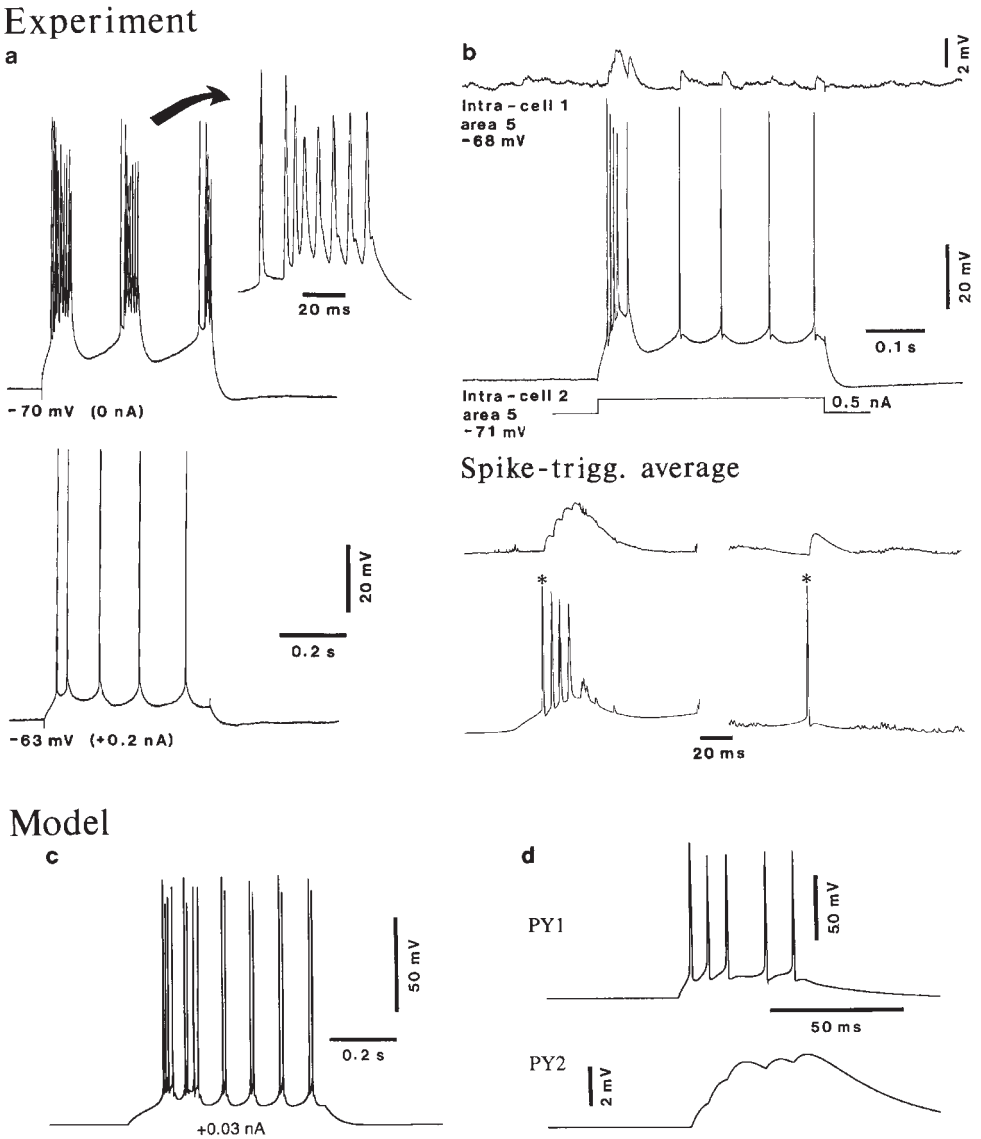

Figure 2. Response properties of neurons in a slab and model neurons. (*a*) Responses of an IB neuron to depolarizing current pulses (0.5 nA) at rest (upper trace) and under slight (+0.2 nA) DC depolarization (bottom trace). A typical burst is expanded (indicated by arrow). (*b*) Burst firing in a presynaptic IB cell results in a larger-amplitude postsynaptic response than that elicited by single spikes. Simultaneous dual intracellular recordings of RS (cell 1) and IB (cell 2) neurons in a slab. Recordings suggest that the two neurons were synaptically connected. A direct depolarization (0.5 nA) applied to the IB cell elicited a high-frequency burst followed by a tail of tonic firing. The burst resulted in a higher-amplitude response in the postsynaptic RS neuron, compared to the EPSPs elicited by single spikes of the IB neuron. The bottom panel depicts spike-triggered (asterisks in IB cell) averages of postsynaptic responses in RS cell; bursts at left, single spikes at right. In this and following figures, membrane potential is indicated. (*c*) Response of a model PY neuron to depolarizing current pulse (0.03 nA). (*d*) Pair of synaptically connected PY cells. Burst of spikes in PY1 neuron resulted in a train of EPSPs in the postsynaptic PY2 cell.

intracellular response that outlasted the duration of the pulse, whose duration increased by slight DC depolarization (Fig. 4*a*, stippled areas), above –65 mV, where $I_{Na(p)}$ is activated (Crill, 1996). With suprathreshold stimulation, the spike after-hyperpolarization shunted the prolonged responses. Therefore, as soon as the neuron became involved in the transmission of input signals and could generate spikes, the amplification of small signals was no longer necessary.

We hypothesized that the depolarizing response, which outlasted the depolarizing current pulse at relatively depolarized V_ms (Fig. 4*a*,*b*), was due to $I_{Na(p)}$ (Stafstrom *et al.*, 1982, 1984, 1985). To study the role of $I_{Na(p)}$ in the generation of active periods, we recorded 24 neurons with pipettes filled with 50 mM solution of QX-314, a quaternary derivative of local anesthetics that nonspecifically antagonizes the $I_{Na(p)}$ (Hille, 1977). The major early effect of QX-314 was the significant decrease in the amplitude of active states (Fig. 5). Later on, 5–10 min after impalement with QX-314-filled pipettes, the neurons lost their ability to generate fast Na^+ spikes and their membrane potential was depolarized by 5–10 mV, most likely due to intracellular blockade of some K^+ currents (Andrade, 1991). The decrease in the depolarizing envelope of active periods occurred within the first tens of second, even before stable intracellular recordings were established. However, in five neurons we were able to obtain stable intracellular recordings immediately after neuronal impalement. In those cases, we calculated the area of depolarization for the first 500 ms for active periods evoked within the first minute of recording and for active periods elicited 7–15 min later (Fig. 5, upper panel). These data showed that, with QX-314-filled pipettes, the area of depolarization

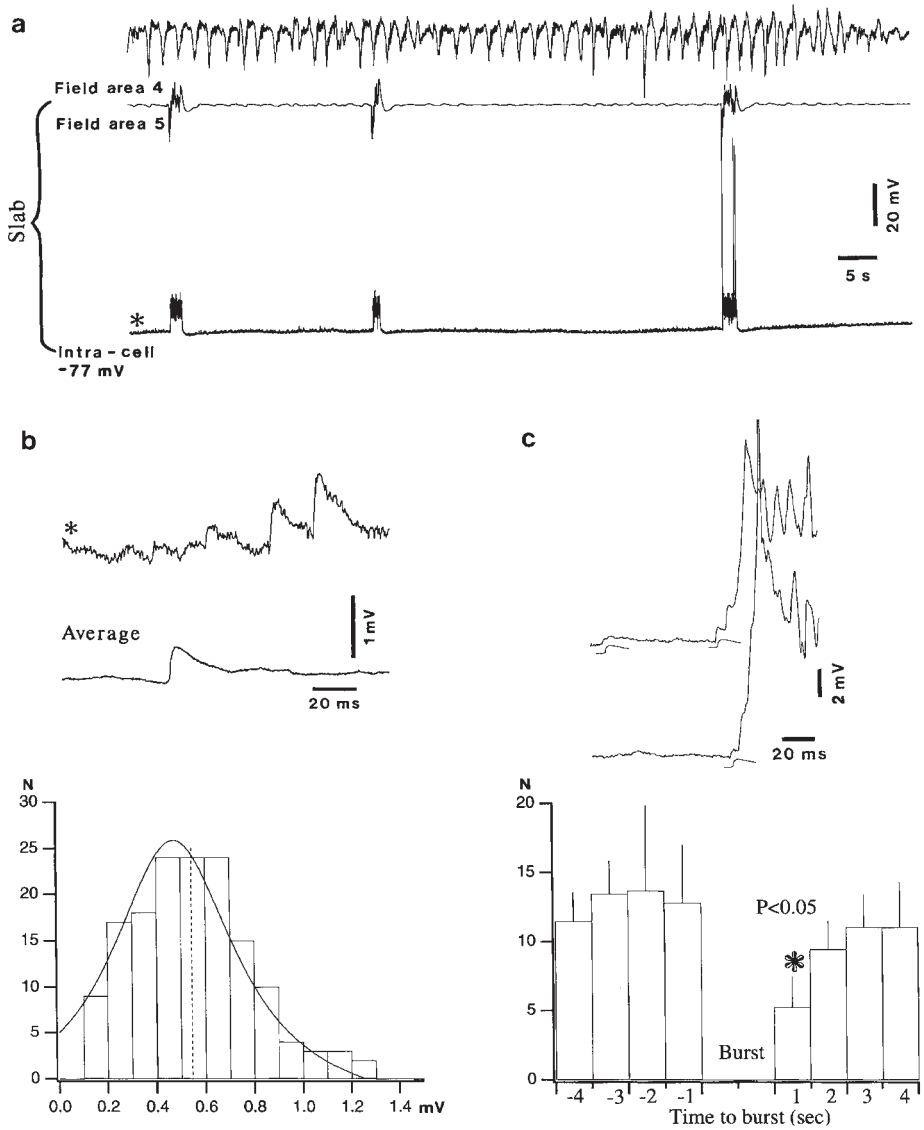

Figure 3. The background neuronal activity in a small slab consists of small depolarizing potentials (SDPs) interrupted by bursts of high-amplitude depolarizing events. (*a*) The three traces represent (from top to bottom) field potentials from area 4 (outside the slab), area 5 (in the slab) and intracellular recording of a neuron within the slab. Part indicated by an asterisk at the extreme left of the intracellular trace is expanded below (in *b*) and shows the presence of SDPs. (*b*) Portion indicated by asterisk in (*a*) and average of 100 SDPs, selected by the maximum of the first derivative of the voltage trace (>4.0 V/s). Below, histogram of amplitude distribution of slow-amplitude depolarizing potentials (SDPs). (*c*) Superimposition of the onset of two bursts from the cellular trace in the top panel (second and third bursts). The average SDP is shown close to individual SDPs. Below, histogram of temporal distribution of SDPs before and after the high-amplitude bursts. The number of SDPs significantly decreased during 1 s after the high-amplitude bursts.

decreased by 30% during long-lasting recordings, when measured from the same membrane potential. In some neurons (n = 4) the depolarizing potential outlasting early EPSP was virtually absent, suggesting that the major part of such outlasting depolarization was mediated by $I_{Na(p)}$. In all neurons recorded with QX-314-filled pipettes, we failed to elicit outlasting depolarizations triggered by short intracellular current pulse, similar to those shown on Figure 4, indicating that $I_{Na(p)}$ is responsible for these depolarizations.

To explore the influence of $I_{Na(p)}$ on the response of the neuron (see above, Fig. 4*a*), we examined the response of a model pyramidal (PY) cell reciprocally connected with a single interneuron (IN) (see Materials and Methods) to short subthreshold current pulses (Fig. 4*c*). From V_m = –63.6 mV, a depolarization produced by a current pulse not only outlasted the duration of the pulse but initiated a transient Na^+ spike. The plot in Figure 4*d* shows the threshold for spike activation in response to EPSPs as a function of the resting V_m for PY neurons with intact (solid line) and blocked (dashed line) $I_{Na(p)}$. A constant reduction of the threshold EPSP amplitude occurred when the $I_{Na(p)}$ was present. This result indicates that randomly occurring miniature EPSPs and $I_{Na(p)}$ might be sufficient to account for the onset of active states of the cortical network.

Propagated Responses in Small Cortical Slabs

Multi-site, field potential and intracellular recordings from small slabs revealed that the onset of spontaneous active periods was systematically delayed at neighboring locations, suggesting that the active periods were propagating; however, the exact place of the origin of spontaneous bursts was difficult to assess. It was possible to elicit such bursts by low-intensity electrical stimuli within the slab. In such cases, the origin of active periods was

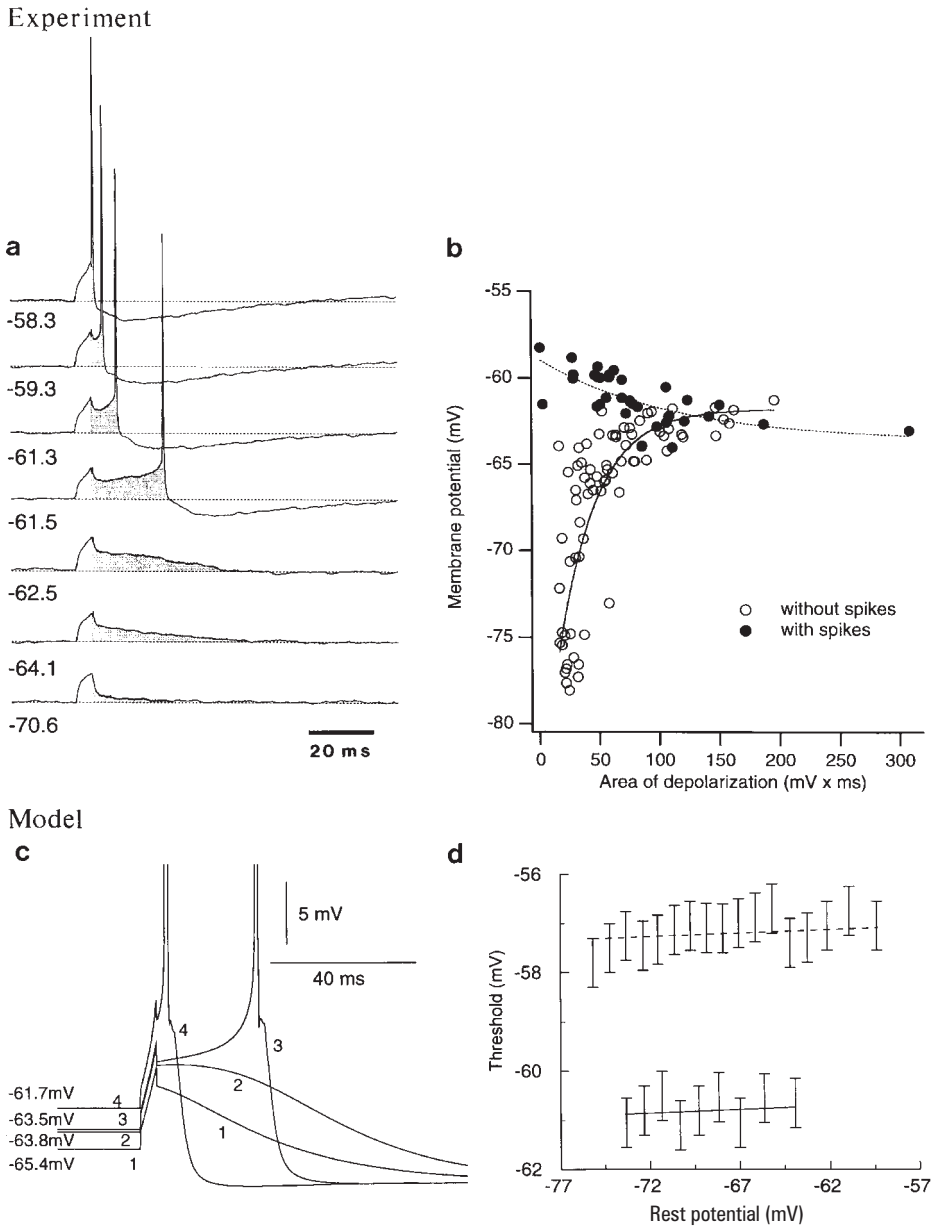

Figure 4. Nonlinear amplification of small depolarizing inputs *in vivo*. (*a*) Short (5 ms) depolarizing current pulses (0.5 nA) were applied at different V_m levels, as indicated in the left part of the figure. As the neuron progressively depolarized (by DC), there was a depolarizing potential that outlasted the current pulse (dotted area) at V_ms more positive than –65 mV, eventually leading to spike generation. The spike AHP truncated this plateau potential. (*b*) The plot indicates the relation between the plateau depolarization area and the V_m. The relation was exponential and an extreme enhancement of the depolarization area occurred as the neuron depolarized above –65 mV (open circles). The occurrence of action potentials at more positive V_ms shortened the depolarization area. (*c*,*d*) Effect of the $I_{Na(p)}$ on response properties of PY cells in network model. (*c*) A PY neuron from a single PY–IN pair is shown at left. Short (5 ms) depolarizing current pulses (0.15 nA) were applied at different V_m levels. The $I_{Na(p)}$ activated for V_ms more depolarized than –63.6 mV was sufficient to initiate an action potential. The depolarizing plateau was terminated by an IN-evoked IPSP.(*d*) EPSPs of varying amplitude were applied to determine a threshold for spike generation at different levels of the PY resting V_m. With intact $I_{Na(p)}$ (solid line), the threshold for action potentials was shifted down by ~4 mV.

close to the site of stimulation. Triple simultaneous intracellular recordings from one IB and two RS neurons in the area 5 slab (see their electrophysiological identification by depolarizing current pulses in Fig. 6) showed that the stimulus elicited an initially depth-negative field potential and compound depolarizing events in all three neurons, with progressively longer latencies in neurons located farther from the stimulating electrode (Fig. 6). The onset of the depolarization was used to calculate the velocity of the propagation. Based on multi-site recordings (n = 5), the propagation velocity was in the range 10–100 mm/s (mean 43.7 ± 27.8 mm/s).

Models of Cortical Networks

Hodgkin–Huxley-type compartmental models were used to represent neurons in the cortical model (see Materials and Methods, and Appendix). The parameters of the model neurons were adjusted to mimic the spike bursting patterns observed in recordings from the slabs (Fig. 2*c*). The synapses between the neurons were based on Markov models of synaptic conductance changes and were also matched to recordings from dual impalements (Fig. 2*d*).

In models of interconnected PY and IN cells (see Materials and Methods), the probability of spontaneous miniature EPSPs at

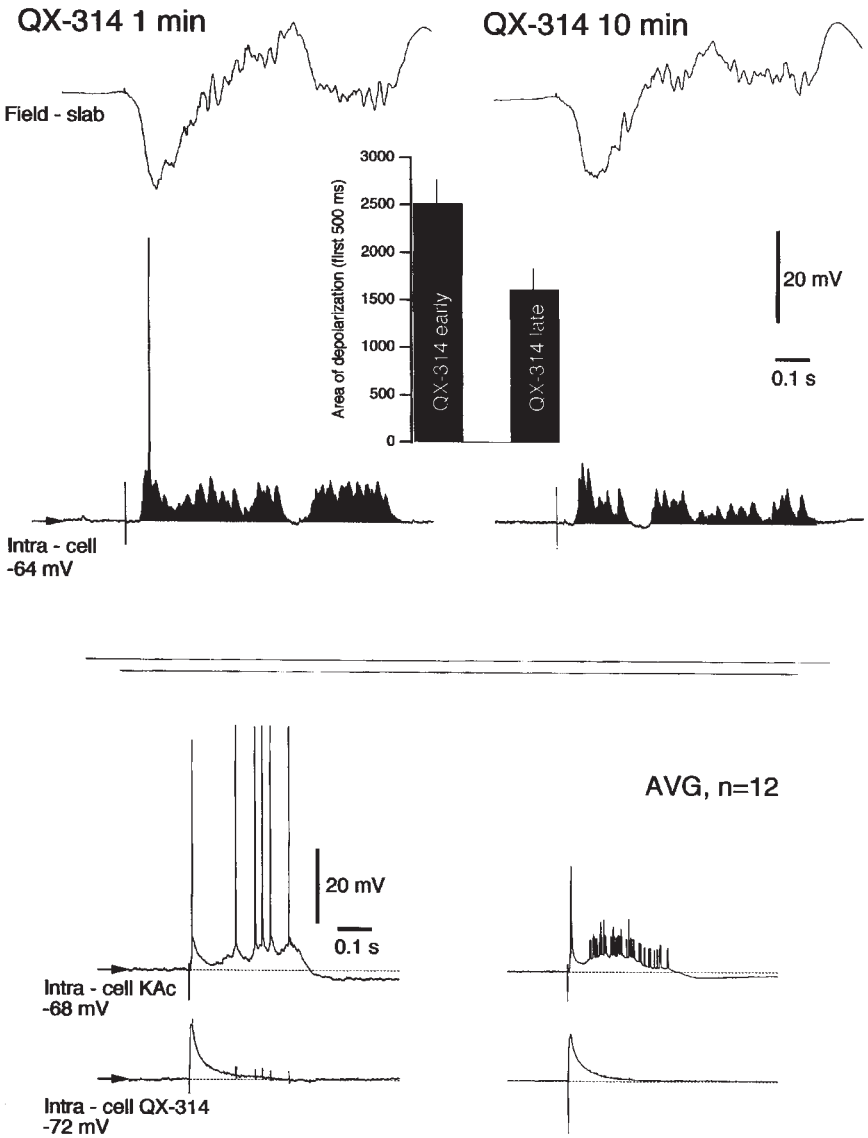

Figure 5. Intracellular effects of QX-314 on active periods in the slab. (*Upper panel*) Field potential and intracellular recordings of two active periods evoked by slightly subthreshold electrical stimulation of the slab. (*Left*) Within the first minute of intracellular recording. (*Right*) Ten minutes later; small (–0.3 nA) DC current was injected in neuron to keep the same membrane potential as at the beginning of recording. (*Bottom*) Simultaneous dual intracellular recordings from two closely located neurons. Upper (control) neuron was recorded with pipette filled with KAc and bottom (tested) neuron was recorded with pipette filled with 50 mM QX-314 diluted in KAc. Note that depolarization outlasting the initial EPSP is almost absent in the neuron recorded with QX-314. Averaged activities from the two neurons are shown on the right.

each synapse started from zero probability at the last Na^+ spike in the presynaptic PY cell, increased during the first few seconds and more slowly reached an asymptote (see Fig. 3). Figure 7*a* shows one PY neuron that was randomly selected from the network of 2 × *N* PY-IN neurons, where *N* was varied from 50 to 2000. When the summation of the miniature EPSPs in one of the PY cells depolarized this cell sufficiently to activate the $I_{Na(p)}$ and to initiate a Na^+ action potential, the activity spread through the network and was maintained by lateral PY–PY excitation and $I_{Na(p)}$ (Fig. 7*b*). A similar mechanism for propagation has been previously described (Golomb and Amitai, 1997); however, this network model only had excitatory neurons and only a single burst lasting ~50 ms was studied. In our model, a weak depression of the excitatory interconnections and activation of the Ca^{2+}-dependent K^+ current led to the termination of activity after a few hundred milliseconds. A similar effect could be achieved by slow inactivation of $I_{Na(p)}$ (Fleidervish and Gutnick, 1996), which, however, was not taken into account in the model. Because any PY neuron could be an initiator of the spontaneous activity and because these events are independent, the total probability of initiation in the network increased with *N*, the number of cells in the network (see below). As a consequence, there was a strong variability in the time intervals between patterns of activity in the small network of 2 × 50 PY–IN cells. In larger networks, the increased number of foci where the activity could be initiated resulted in an increase in the frequency of active periods and less variability in their occurrence (Fig. 7*a*). Note that the probability of spike initiation was smaller for the boundary PY cells, which received a reduced number of intact synapses, so that the active periods were usually initiated far from the network boundaries (see Fig. 7*b*). To test the effects of miniature EPSP size, their amplitude was increased by either 50%

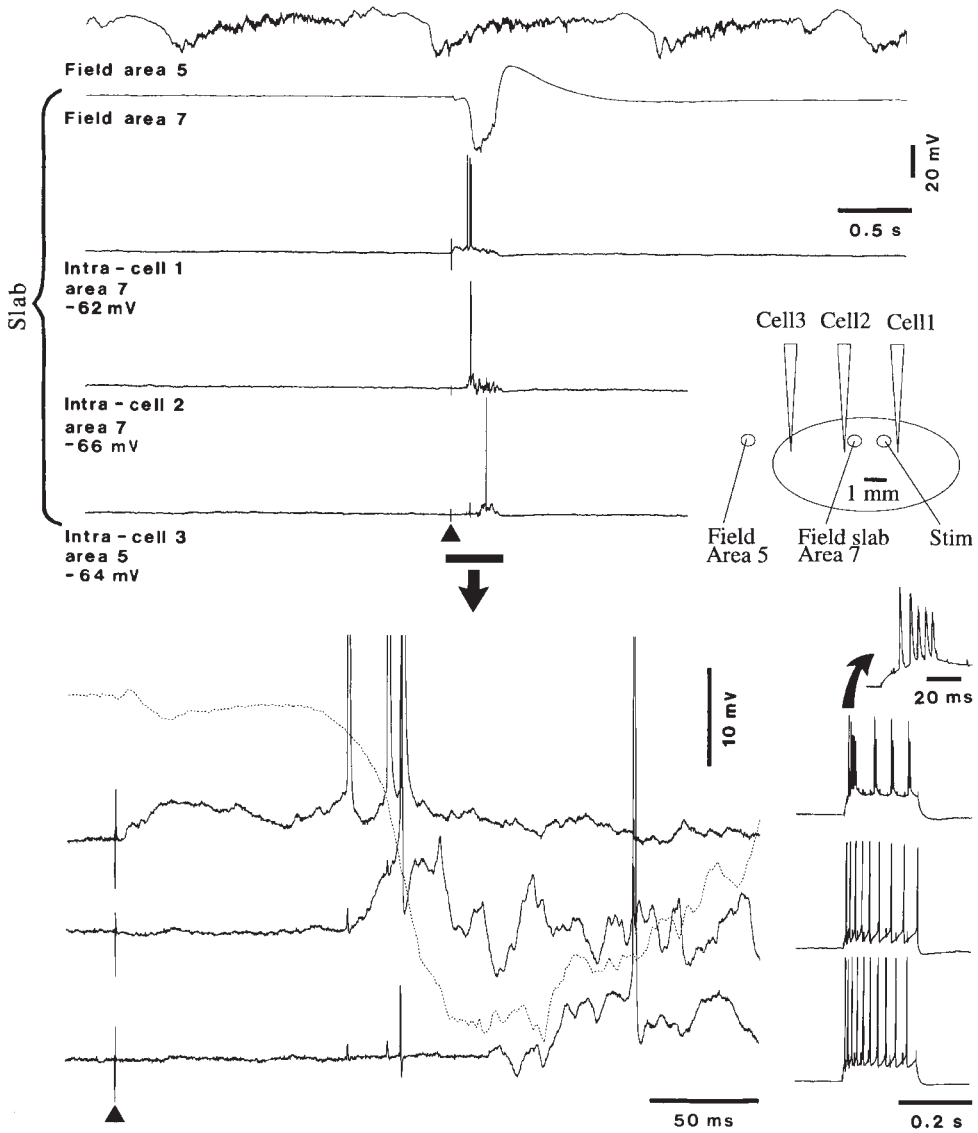

Figure 6. Propagation of evoked activity in the small isolated cortical slab. Simultaneous recordings of field potentials from area 5 (outside the slab) and within the slab in area 7, as well as triple simultaneous intracellular recordings from area 7 slab. The positions of stimulating and recording (field) macroelectrodes as well as micropipettes (cells 1–3) are indicated in the scheme. Low intensity (0.15 mA) stimulation within the slab elicited a field potential and intracellular activities that propagated from the stimulating electrode towards the extremities of the slab. Portion marked by horizontal bar (arrow) is expanded below (small deflections in intracellular recordings are due to capacitive coupling from the simultaneously recorded action potentials in the other neurons). Note the absence of slow oscillation in the field recording from the slab, contrasting with the slow oscillation (~0.7 Hz) recorded from the adjacent area 5. At the bottom right, electrophysiological identification (by depolarizing current pulses, 0.5 nA) of cell 1 (IB neuron; first burst is expanded above) and cells 2–3 (RS neurons).

(top trace in Fig. 7*c*) or 100% (lower trace in Fig. 7*c*). These modifications significantly increased the frequency of spontaneous bursting and in the latter case produced almost periodic oscillations at ~0.5 Hz. This activity is similar to the slow oscillations recorded *in vivo* during slow wave sleep (Steriade *et al.*, 1993c).

Spontaneous Activities in Isolated Cortical Gyri

The relatively low frequency of active states recorded in small isolated slabs, compared to the cortically generated slow oscillation (Steriade *et al.*, 1993c; Contreras and Steriade, 1995), could be due to the relatively small number of neurons in the slab. If so, then an increase in the number of cortical cells in the isolated network may increase and stabilize the frequency of oscillations. To test this hypothesis, we recorded from the isolated suprasylvian gyrus (see Fig. 1*c* and Materials and Methods). A summary of the results obtained in these experiments ($n = 6$) is presented in Figure 8. Field potential recordings from the intact cortex revealed the presence of the cortically generated slow oscillation, accompanied by spindles of thalamic origin (Steriade *et al.*, 1993c; Contreras and Steriade, 1995), in simultaneous recordings from seven cortical sites (Fig. 8*a*). Following the isolation of the suprasylvian gyrus, recording electrodes were placed into the same cortical sites. The frequency of recorded slow activity was similar to the frequency of the slow oscillation, but spindles were absent because thalamocortical projections were interrupted (Fig. 8*b*). An example of intracellular activity recorded from the isolated gyrus is shown in Figure 8*c*. Neurons were hyperpolarized during the depth-positive component of the field potential and were

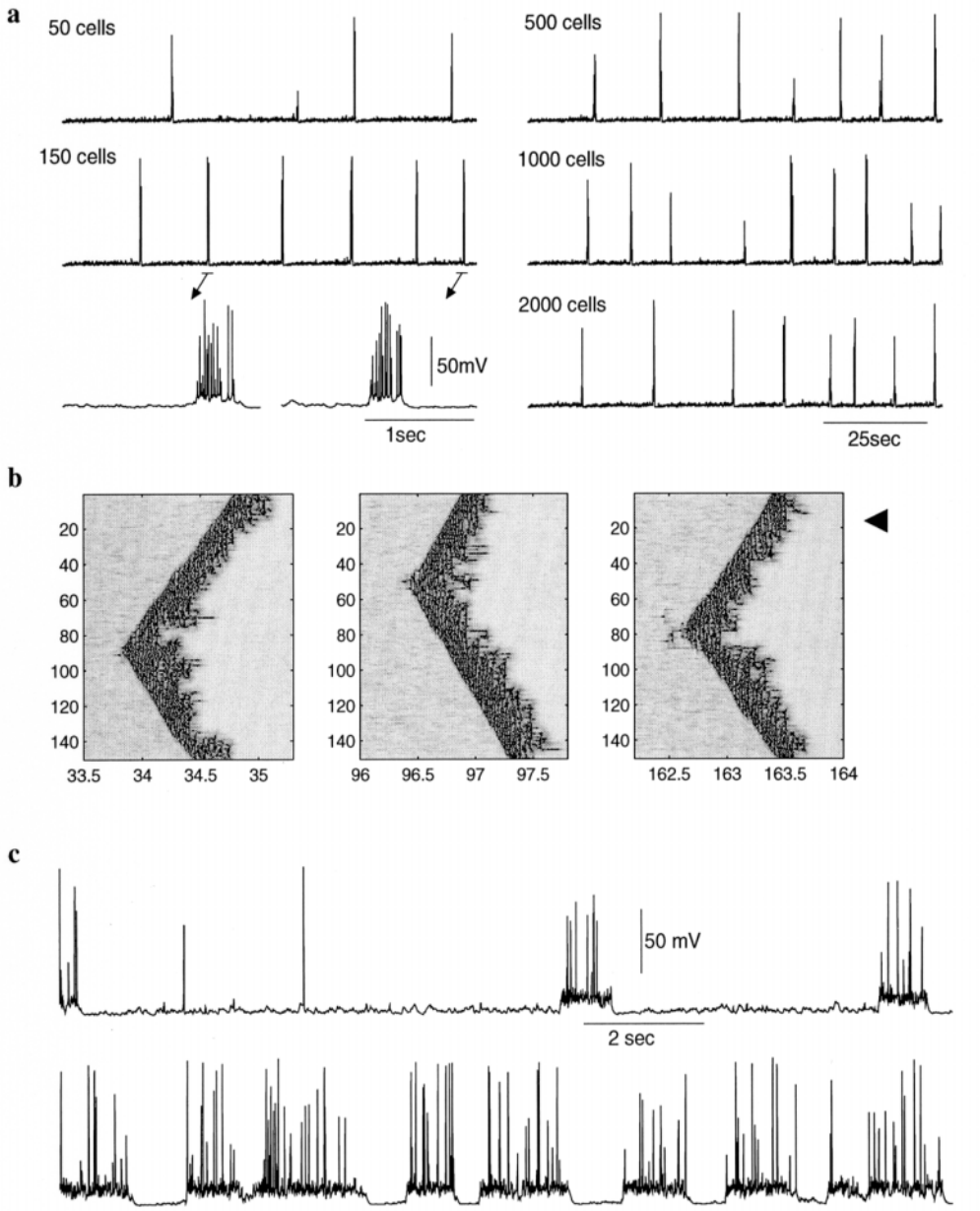

Figure 7. Patterns of spontaneous activity in the network of PY and IN cells. (*a*) In a network with 50 PY–IN pairs, the probability of initiation was relatively low, so the time intervals between bursts varied between 10 and 30 s. An increase of the total number of neurons (up to 2000 PY–IN pairs) raised the probability of initiation and increased and stabilized the frequency of the active periods. Expanded fragments (arrows) show that durations of the active periods are variable. The spike amplitudes varied because of the low sampling rate. (*b*) The activity initiated at different network foci propagated with a constant velocity of ~100 cell/s. Black arrow indicates the PY cell shown in the upper panels. (*c*) Increase (80% at top and 100% at bottom) in the amplitude of miniature EPSPs transformed rare depolarizing events to the quasi-periodic activity at a frequency of ~0.5 Hz.

depolarized, and fired action potentials, during the depth-negative field potentials, as found in intact cortex.

Using a network model with Hodgkin–Huxley-like neurons it was not possible to simulate more than a few thousand cells. To overcome this limitation the mean period of spontaneous bursting and its standard deviation was analytically estimated and compared with *in vivo* data (see Materials and Methods). Figure 9 shows the mean period and standard deviation of bursting as a function of the network size in the computational network model. There was good agreement between the results of Hodgkin–Huxley simulations (filled circles and squares) and the analytical curves. As the network size increased, the mean period of spontaneous bursting reached an asymptote at 1.5–2 s and the coefficient of variation (CV) tended to zero. Thus, the network would reliably burst at a frequency of ~0.5 Hz, within the frequency range of slow oscillations observed in the cortex *in vivo*. For large networks there was no significant difference between results obtained based on a logarithmic rate function (thin lines) and sigmoid rate function (thick lines), which suggests that the scaling behavior is robust to the details of the network model.

In the simulated network model, the asymptotic value of the Poisson rate was chosen higher than that estimated from *in vivo* data. This permitted spontaneous bursting to occur at a reasonable frequency for an extremely small (compared with the real network) model of the PY–IN network. The same high value

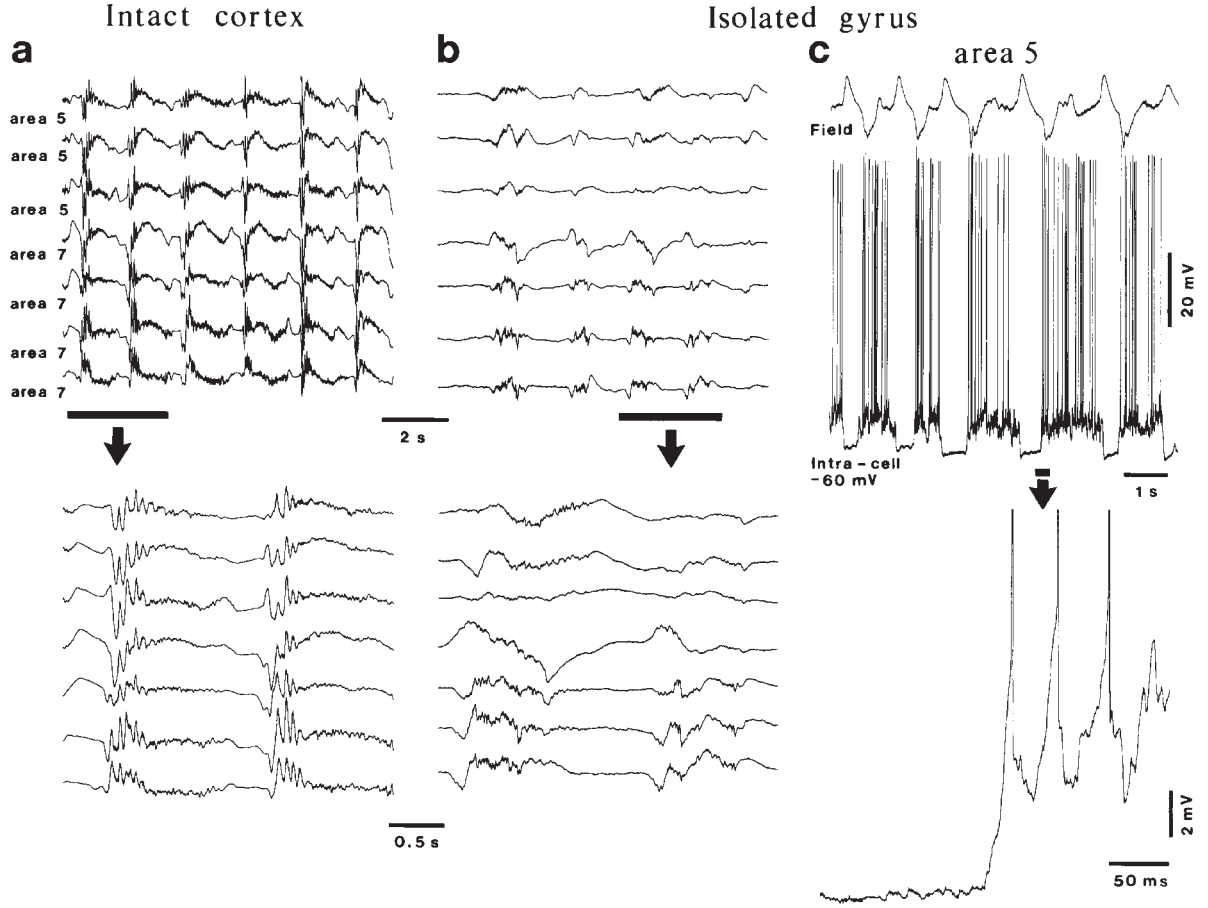

Figure 8. Electrical activity in the isolated gyrus is different from that in slabs but has a similar frequency to that of the slow oscillation in the intact cortical network. (*a*) Each cycle of the slow oscillation in the intact suprasylvian gyrus was followed by a brief spindle-sequence. Electrodes were separated by 1.5 mm. Part marked by horizontal bar is expanded below. (*b*) After preparation of the isolated gyrus, the electrodes were placed in the same positions. The frequency of the slow activity in the isolated gyrus was similar to the frequency of the slow oscillation in the intact cortical network but spindles were absent because of the interruption of thalamocortical connections. (*c*) Similar to the slow oscillation from the intact cortex, the cortical neurons in the isolated gyrus were hyperpolarized during the depth-positive wave of field potentials and depolarized during the depth-negative wave. Slow amplitude depolarizing potentials (SDPs) occurred at the onset of depolarizing phases recorded intracellularly.

of Poisson rate was selected for the analytical calculations presented in Figure 9*a*. Figure 9*b* shows similar curves calculated for parameters of the miniature events estimated directly from *in vivo* data. In particular, the function $\mu(t)$ for the rate of miniature events as function of time was found by fitting the histogram in Figure 3*c*. The total number of cells was estimated to be 10×10^6 in the cortical slab and ~100×10^6 in the isolated gyrus. The number of cells in the isolated slab was close to the minimal number that the model predicted should be needed to generate activity. The mean interburst interval for the slab was 24 s and CV = 0.87. Further reduction of the slab size led to a dramatic decrease of the average frequency of burst initiation and increase in the variability of the interburst intervals. As the number of neurons and synapses in the network increased, the frequency of active periods increased toward an asymptotic value. For an isolated gyrus the mean period of bursting was predicted to be 4.9 s with CV = 0.47. For 10^9 neurons in a 100 cm^2 region of cortex, the predicted frequency of spontaneous bursting was ~0.5 Hz and the CV < 0.3 (see Fig. 9*b*), in good agreement with *in vivo* recordings. The frequency was nearly independent of size for larger cortical regions because there is a minimum recovery time following a depolarizing event (Fig. 3*c*).

Discussion

The level of activity and properties of neurons in a neocortical slab depend on its size. Intracellular and field potential recordings in isolated small neocortical slabs have revealed several differences from intact cortex: (i) the percentage of IB neurons (near 40%) is double that reported in the intact cortex under anesthesia; (ii) the absence of spontaneously occurring slow oscillation stands in contrast to the presence of this oscillation recorded simultaneously from the intact cortex; and (iii) an increased number of connected cells in larger isolated gyri allows the occurrence of the slow oscillation, similar to that seen in the intact cortex.

The greatly increased incidence of IB neurons may be ascribed to the reduction in synaptic activity within small slabs. One of the documented properties of IB neurons is their transformation to an RS-type pattern by synaptic activation and depolarization during brainstem-induced arousal (Steriade *et al.*, 1993a), mainly due to the activation of metabotropic glutamate and cholinergic receptors (Wang and McCormick, 1993). In recent intracellular recordings during natural states of vigilance in behaving cats, the incidence of IB neurons was <5% (Steriade *et al.*, 1999), consistent with the hypothesis proposed above.

Whereas action potentials were absent between the large-

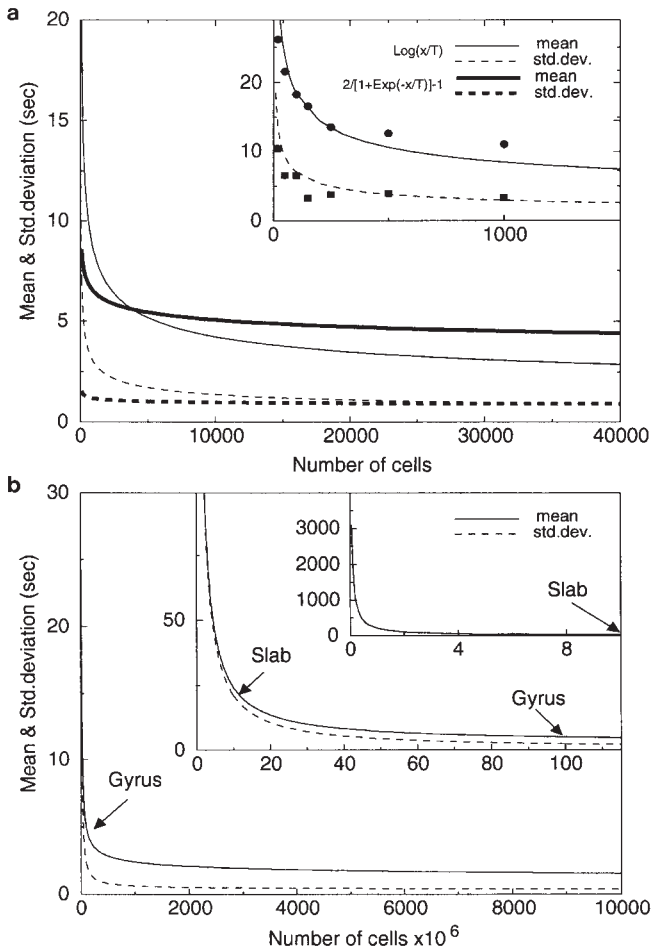

Figure 9. Estimated mean T and standard deviation σ of interburst intervals for networks of different size. (*a*) Analytical model (curves) and data from simulated Hodgkin–Huxley model with different number of cells (circles: mean; squares: standard deviation). Critical number of miniature EPSPs n and time δt used in analytical calculations were taken from the computational model: $\delta t = 27$ ms, $n = 13$. Thinner lines correspond to the logarithmic rate function and thicker lines correspond to the sigmoid rate function (see Appendix). (*b*) Analytical curves based on *in vivo* data: $\delta t = 22$ ms, $n = 9$. Estimated mean of interburst intervals for a slab (~10×10^6 neurons) is 24 s (SD 21 s) and for a gyrus (~100×10^6 neurons) the mean is 4.9 s (SD 2.3 s).

amplitude depolarizing events, separated by very long periods of neuronal silence, SDPs (probably minis) occurred at high frequencies. In recent studies conducted *in vivo* and in cultures, the TTX-resistant minis were found to be sensitive to $GABA_A$ or AMPA antagonists (Paré *et al.*, 1997) and were implicated in the maintenance of dendritic spines (McKinney *et al.*, 1999). The spontaneously occurring SDPs and the non-linear amplification of small amplitude signals contribute to the generation of large depolarizing events, occasionally superimposed by action potentials, as shown here in isolated slabs. It is likely that the depolarization of neuronal soma by subthreshold current pulses (see Fig. 4) activates $I_{Na(p)}$, which occurs ~10 mV more negative than the transient Na^+ current (Stafstrom *et al.*, 1982, 1985; Thomson *et al.*, 1988). The AHP following the action potentials results in a large conductance increase that significantly decreases the slow regenerative $I_{Na(p)}$ (Schwindt *et al.*, 1988). As soon as action potentials are generated, and even more so with spike-bursts generated by IB neurons, the non-linear amplification is shunted by AHPs and feedback synaptic activity. Computer simulations support the hypothesis that intrinsic currents amplify small incoming signals during the silent periods.

The activity in the slab propagated with a velocity that was in a range similar to that previously reported from studies on cell cultures prepared from the cortex of embryonic rats (Maeda *et al.*, 1995) and in disinhibited slices (Chagnac-Amitai and Connors, 1989). EPSPs reaching the neurons at a relatively hyperpolarized level do not elicit spikes but activate $I_{Na(p)}$, which may lead to spike generation delayed by 30–50 ms from the EPSP onset. Under these conditions, only a few synapses are needed to delay the response by hundreds of milliseconds, as in Figure 4. Thus, during the silent states of the isolated slabs as well as during the prolonged hyperpolarizations characterizing the state of sleep or anesthesia, the SDPs, delayed spiking and mutual facilitatory connections are responsible for the propagation at the onset of active periods. This propagation may also be mediated by the abundant intracortical connections within the cat suprasylvian gyrus, as shown both morphologically (Avendaño *et al.*, 1988) and electrophysiologically (Amzica and Steriade, 1995b). Similar horizontal projections of pyramidal axons, spanning up to 8 mm, are found in the visual cortex (Gilbert, 1992) as well as in other areas. The coherent membrane potential fluctuations recorded from neocortical neurons during the slow (<1 Hz) oscillation (Amzica and Steriade, 1995a,b) and other activities (Lampl *et al.*, 1999) are mediated by the same intracortical connections because these slow rhythms survive thalamectomy (Steriade *et al.*, 1993c).

Although large depolarizations were commonly found spontaneously or could be elicited by stimulating the slab, spontaneous slow oscillations were absent in small slabs; however, slow oscillations were present in larger isolated cortical territories, covering a full gyrus. Thus, the occurrence and maintenance of spontaneous oscillations may require a minimal number of neurons. Assuming a columnar density of ~160 000 neurons/mm^2 in neocortex, >10×10^6 neurons (for a slab of 6 mm × 10 mm size) and >50×10^6 neurons (for an isolated gyrus of 30 mm × 20 mm size) were needed. The analytical model for the occurrence of spontaneous activity (see Materials and Methods) predicted that the frequency of spontaneous oscillations should be stabilized near the frequency level of slow cortical oscillations for networks containing more than ~100×10^6 neurons (see Fig. 9*b*). In network models of thalamic reticular neurons, the propensity for self-sustained oscillations also depended critically on the number of synapses in the network (Bazhenov *et al.*, 1999). Thus, there may be a general principle regarding the minimum size of network connectivity needed to achieve spontaneous, large-scale coherent activity in thalamocortical systems. In the model, this size depended on many parameters such as the average number of synapses on one cell and the probability and the amplitude of miniature EPSPs for each synapse, which need to be more accurately estimated from direct measurements (Murthy *et al.*, 2000).

In the above scenario, slow wave activity is driven by the spontaneously occurring coincidence of small depolarizing events, such as miniature excitatory postsynaptic potentials, or minis. Spontaneous miniature synaptic activity is caused by action-potential-independent release of transmitter vesicles and is regulated at the level of single synapses (Salin and Prince, 1996; Paré *et al.*, 1997). The frequency of spontaneous miniature synaptic events increases with the probability of evoked release in cortical neurons (Prange and Murphy, 1999). Thus, the synapses with the highest probability of release (Murthy *et al.*,

1997) should make the largest contribution to initiating an action potential in a neuron. Glutamate application at synapses between hippocampal neurons produces long-term potentiation of the frequency of spontaneous miniature synaptic currents (Malgaroli and Tsien, 1992), which suggests that the synapses with the highest rates of spontaneous miniature synaptic currents are the most likely to have been recently potentiated. During sleep the initiation of spikes could therefore occur in neurons with the largest number of recently potentiated synapses. If these spontaneously occurring minis are amplified by the intrinsic currents in dendrites, it may not take a large number of coincident events to initiate a spike. The spiking neuron would further need to recruit additional neurons connected to it; the ones nearest to threshold would be those depolarized as a consequence of minis, so that the recruited network would preferentially include cells that had been recently potentiated. Other factors that would influence recruitment include multiple synaptic boutons (Markram *et al.*, 1997), spike bursting, which may itself further potentiate recently activated afferent synapses by virtue of the burst in the postsynaptic cell (Paulsen and Sejnowski, 2000), and efferent synapses that were recently potentiated. This interpretation is consistent with the observation that unilateral somatosensory stimulation prior to sleep in humans increases the power of low-frequency oscillations, but only on the side of the cortex that received stimulation (Kattler *et al.*, 1994).

The model shows how a single neuron could recruit an avalanche of activity in a selected subset of a previously silent recurrent network of cortical neurons and serve as the nucleus for the spread of activity to neighboring cortical territory. This sequence of events should start from a basal state of inactivity, when the silent cortex is primed for the type of 'sharp wave' activity that has been observed in the hippocampus (Buzsáki, 1986). Thus, the slow oscillations characteristic of the cortex during sleep may be an emergent property of large cortico-thalamic systems that, surprisingly, may be triggered by activity originating in single neurons. One of the predictions of this model is that the frequency of slow oscillations should be temperature dependent, since the rate of miniature synaptic activity (Barrett *et al.*, 1978), and hence the probability of reaching threshold, should increase with temperature. The temperature dependence of the frequency of slow oscillations observed in hibernating hamsters is compatible with this prediction (Deboer, 1998).

The relatively simple cortical network models examined here may not include features of the cerebral cortex needed to fully understand the genesis of slow cortical oscillations. Other explanations may also be compatible with the experimental data; nonetheless, the data and models form a consistent picture and further experimental studies are needed to test the predictions and refine the proposed mechanisms.

Notes

This research was supported by the Medical Research Council of Canada, the Howard Hughes Medical Institute and the Human Frontier Science Program.

Address correspondence to Professor M. Steriade, Laval University, School of Medicine, Laboratory of Neurophysiology, Quebec, Canada G1K 7P4. Email: mircea.steriade@phs.ulaval.ca.

References

Achermann P, Borbély A (1997) Low-frequency (<1 Hz) oscillations in the human sleep EEG. Neuroscience 81:213–222.

Alzheimer C, Schwindt PC, Crill WE (1993) Modal gating of Na^+ channels as a mechanism of persistent Na^+ current in pyramidal neurons from rat and cat sensorimotor cortex. J Neurosci 13:660–673.

Amzica F, Steriade M (1995a) Short- and long-range neuronal synchronization of the slow (<1 Hz) cortical oscillation. J Neurophysiol 73:20–38.

Amzica F, Steriade M (1995b) Disconnection of intracortical synaptic linkages disrupts synchronization of a slow oscillation. J Neurosci 15:4658–4677.

Amzica F, Steriade M (1997) The K-complex: its slow (<1 Hz) rhythmicity and relation with delta waves. Neurology 49:952–959.

Andrade, R. (1991) Blockade of neurotransmitter-activated K^+ conductance by QX-314 in the rat hippocampus. Eur J Pharmacol 199:259–62.

Avendaño C, Rausell E, Perez-Aguilar D, Isorna S (1988) Organization of the association cortical afferent connections of area 5: a retrograde tracer study in the cat. J Comp Neurol 278:1–33.

Avoli M (1986) Inhibitory potentials in neurons of the deep layers of the *in vitro* neocortical slice. Brain Res 370:165–170.

Barrett EF, Barrett JN, Botz D, Chang DB, Mahaffey D (1978) Temperature-sensitive aspects of evoked and spontaneous transmitter release at the frog neuromuscular junction. J Physiol 279:253–73

Bazhenov M, Timofeev I, Steriade M, Sejnowski TJ (1998) Computational models of thalamocortical augmenting responses. J Neurosci 18:6444–6465.

Bazhenov M, Timofeev I, Steriade M, Sejnowski TJ (1999) Self-sustained rhythmic activity in the thalamic reticular nucleus mediated by depolarizing $GABA_A$ receptor potentials. Nature Neurosci 2:168–174.

Burns BD (1950) Some properties of the cat's isolated cerebral cortex. J Physiol 111:50–68.

Buzsáki G (1986) Hippocampal sharp waves: their origin and significance. Brain Res 398:242–252.

Chagnac-Amitai Y, Connors BW (1989) Horizontal spread of synchronized activity in neocortex and its control by GABA-mediated inhibition. J Neurophysiol 61:747–758.

Connors BW, Gutnick MJ, Prince DA (1982) Electrophysiological properties of neocortical neurons *in vitro*. J Neurophysiol 48:1302–1320.

Connors BW, Malenka RC, Silva LR (1988) Two inhibitory postsynaptic potentials, and $GABA_A$ and $GABA_B$ receptor-mediated responses in neocortex of rat and cat. J Physiol 406:443–368.

Contreras D, Steriade M (1995) Cellular basis of EEG slow rhythms: a study of dynamic corticothalamic relationships. J Neurosci 15:604–622.

Crill W. E. (1996) Persistent sodium current in mammalian central neurons. Annu Rev Physiol 58: 349–62.

Deboer T (1998) Brain temperature dependent changes in the electroencephalogram power spectrum of humans and animals. J Sleep Res 7:254–262.

Destexhe A, Paré D (1999) Impact of network activity on the integrative properties of neocortical pyramidal neurons *in vivo*. J Neurophysiol 81:1531–1542.

Echlin FA, Arnett V, Zoll J (1952) Paroxysmal high voltage discharges from isolated and partially isolated human and animal cerebral cortex. Electroenceph Clin Neurophysiol 4:147–164.

Fatt P, Katz B (1952) Spontaneous subthreshold activity at motor nerve endings. J Physiol 117:109–128.

Fleidervish IA, Gutnick MJ (1996) Kinetics of slow inactivation of persistent sodium current in layer V neurons of mouse neocortical slices. J Neurophysiol 76:2125–2130.

Galarreta M, Hestrin S (1998) Frequency-dependent synaptic depression and the balance of excitation and inhibition in the neocortex. Nature Neurosci 1:587–594.

Gilbert CD (1992) Horizontal integration and cortical dynamics. Neuron 9:1–13.

Golomb D, Amitai Y (1997) Propagating neuronal discharges in neocortical slices: computational and experimental study. J Neurophysiol 78:1199–1211.

Gray CM, McCormick DA (1996) Chattering cells: superficial pyramidal neurons contributing to the generation of synchronous oscillations in the visual cortex. Science 274:109–113.

Gupta A, Wang, Y, Markram H (2000) Organizing principles for a diversity of GABAergic interneurons and synapses in the neocortex. Science 287:273–278

Hille B (1977) Local anesthetics: hydrophilic and hydrophobic pathways for the drug-receptor reaction. J Gen Physiol 69:497–515.

Kay AR, Sugimori M, Llinás R (1998) Kinetic and stochastic properties of

a persistent sodium current in mature guinea pig cerebellar Purkinje cells. J Neurophysiol 80:1167–1179.
Kattler H, Dijk DJ, Borbély AA (1994) Effect of unilateral somatosensory stimulation prior to sleep on the sleep EEG in humans. J Sleep Res 3:159–164.
Lampl I, Reichova I, Ferster D (1999) Synchronous membrane potential fluctuations in neurons of the cat visual cortex. Neuron 22:361–374.
Llinás R, Ribary U (1993) Coherent 40-Hz oscillation characterizes dream state in humans. Proc Natl Acad Sci USA 90:2078–2081.
Maeda E, Robinson HPC, Kawana A (1995) The mechanisms of generation and propagation of synchronized bursting in developing networks of cortical neurons. J Neurosci 15:6834–6845.
Mainen ZF, Sejnowski TJ (1996) Influence of dendritic structure on firing pattern in model neocortical neurons. Nature 382:363–366.
Malgaroli A, Tsien RW (1992) Glutamate-induced long-term potentiation of the frequency of miniature synaptic currents in cultured hippocampal neurons. Nature 357:134–139.
Markram H (1997) A network of tufted layer 5 pyramidal neurons. Cereb Cortex 7:523–533.
Markram H, Lubke J, Frotscher M, Sakmann B (1997) Regulation of synaptic efficacy by coincidence of postsynaptic APs and EPSPs. Science 275:213–215.
McCormick DA, Connors BW, Lighthall JW, Prince DA (1985) Comparative electrophysiology of pyramidal and sparsely spiny stellate neurons of the neocortex. J Neurophysiol 54:782–806.
McKinney RA, Capgna M, Dürr R, Gähwiler BH, Thompson SM (1999) Miniature synaptic events maintain dendritic spines via AMPA receptor activation. Nature Neurosci 2:44–49.
Murthy VN, Sejnowski TJ Stevens CF (1997) Heterogeneous release properties of visualized individual hippocampal synapses. Neuron 18:599–612.
Murthy VN, Sejnowski TJ, Stevens C (2000) Dynamics of dendritic calcium transients evoked by quantal release at excitatory hippocampal synapses. Proc Natl Acad Sci USA 97:901–906.
Nuñez A, Amzica F, Steriade M (1993) Electrophysiology of cat association cortical cells *in vivo*: intrinsic properties and synaptic responses. J Neurophysiol 70:418–430.
Paré D, Lebel E, Lang EJ (1997) Differential impact of miniature synaptic potentials on the somata and dendrites of pyramidal neurons *in vivo*. J Neurophysiol 78:1735–1739.
Paré D, Shink E, Gaudreau H, Destexhe A, Lang EJ (1998) Impact of spontaneous synaptic activity on the resting properties of cat neocortical neurons *in vivo*. J Neurophysiol 79:1450–1460.
Paulsen, O and Sejnowski TJ (2000) Natural patterns of activity and long-term synaptic plasticity. Curr Opin Neurobiol 10:172–179.
Prange O, Murphy TH (1999) Correlation of miniature synaptic activity and evoked release probability in cultures of cortical neurons. J Neurosci 19:6427–6438.
Redman S (1990). Quantal analysis of synaptic potentials in neurons of the central nervous system. Physiol Rev 70:165–198.
Salin PA, Prince DA (1996) Spontaneous $GABA_A$ receptor-mediated inhibitory currents in adult rat somatosensory cortex. J Neurophysiol 75:1573–1588.
Schwindt PC, Spain WJ, Crill WE (1988) Influence of anomalous rectifier activation on afterhyperpolarization of neurons from cat sensorimotor cortex *in vitro*. J Neurophysiol 59:468–481.
Schwindt PC, O'Brien JA, Crill WE (1997) Quantitative analysis of firing properties of pyramidal neurons from layer 5 of rat sensorimotor cortex. J Neurophysiol 77:2484–2498.
Stafstrom CE, Schwindt PC, Crill WE (1982) Negative slope conductance due to a persistent subthreshold sodium current in cat neocortical neurons *in vitro*. Brain Res. 236:221–226.
Stafstrom CE, Schwindt PC, Flatman JA, Crill WE (1984) Properties of subthreshold response and action potential recorded in layer V neurons from cat sensorimotor cortex *in vitro*. J Neurophysiol 52:244–263.
Stafstrom CE, Schwindt PC, Chubb MC, Crill WE (1985) Properties of persistent sodium conductance and calcium conductance of layer V neurons from cat sensorimotor cortex *in vitro*. J Neurophysiol 53:153–170.
Steriade M (1997) Synchronized activities in coupled oscillators in the cerebral cortex and thalamus at different levels of vigilance. Cereb Cortex 7:583–604.
Steriade M, Amzica F, Nuñez A (1993a) Cholinergic and noradrenergic modulation of the slow (~0.3 Hz) oscillation in neocortical cells. J Neurophysiol 70:1385–1400.
Steriade M, McCormick DA, Sejnowski TJ (1993b) Thalamocortical oscillations in the sleeping and aroused brain. Science 262:679–685.
Steriade M, Nuñez A, Amzica F (1993c) Intracellular analysis of relations between the slow (<1 Hz) neocortical oscillation and other sleep rhythms of the electroencephalogram. J Neurosci 13:3266–3283.
Steriade M, Amzica F, Contreras D (1996) Synchronization of fast (30–40 Hz) spontaneous cortical rhythms during brain activation. J Neurosci 16:392–417.
Steriade M, Timofeev I, Dürmüller N, Grenier F (1998a) Dynamic properties of corticothalamic neurons and local cortical interneurons generating fast rhythmic (30–40 Hz) spike bursts. J Neurophysiol 79:483–490.
Steriade M, Timofeev I, Grenier F, Dürmüller N (1998b) Role of thalamic and cortical neurons in augmenting responses and self-sustained activity: dual intracellular recordings *in vivo*. J Neurosci 18:6425–6443.
Steriade M, Timofeev I, Grenier F (1999) Intracellular activity of various neocortical cell-classes during the natural wake-sleep cycle. Soc Neurosci Abstr 25:1661.
Stevens CF (1993) Quantal release of neurotransmitter and long-term potentiation. Cell 72:55–63.
Thomson AM (1997) Activity-dependent properties of synaptic transmission at two classes of connections made by rat neocortical pyramidal axons *in vitro*. J Physiol 502:131–147.
Thomson AM, Deuchars J (1997) Synaptic interactions in neocortical local circuits: dual intracellular recordings *in vitro*. Cereb Cortex 7:510–522.
Thomson AM, Girdlesone D, West DC (1988) Voltage-dependent currents prolong single-axon postsynaptic potentials in layer III pyramidal neurons in rat neocortical slices. J Neurophysiol 60:1896–1907.
Thomson AM, West DC, Hahn J, Deuchars J (1996) Single axon IPSPs elicited in pyramidal cells by three classes of interneurones in slices of rat neocortex. J Physiol 496:81–102.
Tsodyks MV, Markram H (1997) The neural code between neocortical pyramidal neurons depends on neurotransmitter release probability. Proc Natl Acad Sci USA 94:719–723.
Wang Z, Cormick DA (1993) Control of firing mode of corticotectal and corticopontine layer V burst-generating neurons by norepinephrine, acetylcholine and 1*S*,3*R*-ACPD. J Neurosci 13:2199–2216.
Watts DJ, Strogatz SH (1998) Collective dynamics of 'small-world' networks. Nature 393:440–442.

Appendix

The membrane potentials of PY and IN cells are governed by the equations

$$C_m dV_D/dt = -g_L(V_D - E_L) - g(V_D - V_S) - I_D - I^{syn} \qquad (A1)$$
$$g(V_S - V_D) = - I_S$$

where C_m is the membrane capacitance and g_L is the leakage conductance of the dendritic compartment, E_L is the reversal potential, V_D and V_S are the membrane potentials of the dendritic and axo-somatic compartments, I_D and I_S are the sums of active intrinsic currents in axo-somatic and dendritic compartments, I^{syn} is a sum of synaptic currents and g is the conductance between axo-somatic and dendritic compartments. The area of an axo-somatic compartment was 10^{-6} cm^2 for both PY and IN cells and the ratio between areas of the dendritic and axo-somatic compartments was $\rho = 165$ for PY cells and $\rho = 50$ for IN cells. The model included a high density of the fast Na^+ channels, I_{Na}, in axo-somatic compartment and a low density in the dendritic compartment. A fast potassium K^+ current, I_K, and persistent Na^+ current, $I_{Na(p)}$, were present in the axo-somatic compartment. A slow, voltage-dependent K^+ current, I_{Km}, a slow, Ca^{2+}-dependent K^+ current, $I_{K(Ca)}$, a high-threshold Ca^{2+} current, I_{Ca}, and a persistent Na^+ current, $I_{Na(p)}$, were included in the dendritic compartment. The passive parameters were $C_m = 0.75$ $\mu F/cm^2$, $g_L = 0.033$ mS/cm^2, $E_L = -70$ mV, $g = 10$ MΩ.

Intrinsic Currents

The ionic currents are described by the equation:

$$I_{D(S)} = q_T g_j m^M h^N (V - E_j) \quad \text{(A2)}$$

where the maximal conductances are g_{Na} = 3000 mS/cm^2, g_K = 200 mS/cm^2, $g_{Na(p)}$ = 0.06–0.07 mS/cm^2 for axo-somatic compartment; g_{Na} = 1.5 mS/cm^2 , g_{Km} = 0.01 mS/cm^2, $g_{Na(p)}$ = 0.06–0.07 mS/cm^2, $g_{K(Ca)}$ = 0.3 mS/cm^2, g_{Ca} = 0.01–0.015 mS/cm^2 for dendritic compartment. For all cells E_{Na} = 50 mV, E_K = -95 mV, E_{Ca} = 140 mV.

The gating variables $m(t)$, $h(t)$ for all of the ionic currents follow:

$$dm/dt = [m_\infty(V) - m]/\tau_m(V), \quad dh/dt = [h_\infty(V) - h]/\tau_h(V) \quad \text{(A3)}$$

$I_{Na(p)}$: $M = 1$, $N = 0$, $q_T = 1$, $m_\infty = 1/\{1 + \exp[-(V + 42)/5]\}$, $\tau_m = 0.2$

$I_{K(Ca)}$: $M = 1$, $N = 0$, $q_T = 2.95$, $m_\infty = [Ca]/([Ca] + 2)$, $\tau_m = 34/([Ca]+2)$

I_{Km}: $M = 1$, $N = 0$, $q_T = 2.95$, $m_\infty = a/(a + b)$, $\tau_m = 0.34/(a + b)$, $a = 0.001(V + 30)/\{1 - exp[-(V + 30)/9]\}$, $b = -0.001\ (V + 30)/\{1 - exp[(V + 30)/9]\}$

I_{Ca}: $M = 2$, $N = 1$, $q_T = 2.95$, $m_\infty = a/(a + b)$, $\tau_m = 0.34/(a + b)$, $a = 0.055(-27 - V)/\{\exp[(-27 - V)/3.8] - 1\}$, $b = 0.94\exp[(-75 - V)/17]$, $h_\infty = c/(c + d)$, $\tau_h = 0.34/(c + d)$, $c = 0.000457 \exp[(-13 - V)/50]$, $d = 0.0065/\{\exp[(-V - 15)/28] + 1\}$

I_K: $M = 1$, $N = 0$, $q_T = 2.95$, $m_\infty = a/(a + b)$, $\tau_m = 0.34/(a + b)$, $a = 0.02(V - 25)\ (1 - \exp[-(V - 25)/9])$, $b = -0.002(V - 25)/\{1 - \exp[(V - 25)/9]\}$

I_{Na}: $M = 3$, $N = 1$, $q_T = 2.95$, $m_\infty = a/(a + b)$, $\tau_m = 0.34/(a + b)$, $a = 0.182(V + 25)/\{1 - \exp\{-(V + 25)/9]\}$ if $|V - 10|/35 > 10^{-6}$ and $a = 1.638$ if $|V - 10|/35 < 10^{-6}$, $b = 0.124[-(V + 25)]/\{1 - \exp[(V + 25)/9]\}$ if $|V - 10|/35 > 10^{-6}$ and $b = 1.116$ if $|V - 10|/35 < 10^{-6}$, $h_\infty = 1/\{1 + \exp[(V + 55)/6.2]\}$, $\tau_h = 0.34/(c + d)$, $c = 0.024(V + 40)/\{1 - \exp[-(V + 40)/5]\}$ if $|V - 10|/50 > 10^{-6}$ and $c = 0.12$ if $|V - 10|/75 < 10^{-6}$, $d = 0.0091(V - 85)/\{1 - \exp[-(V - 85)/5]\}$ if $|V - 10|/75 > 10^{-6}$ and $c = 0.0455$ if $|V - 10|/50 < 10^{-6}$.

For each cell the Ca^{2+} dynamic were described by a simple first-order model:

$$d[Ca]/dt = -A\ I_{Ca} - ([Ca] - [Ca_\infty])/\tau \quad \text{(A4)}$$

where $[Ca_\infty] = 2.4 \times 10^{-4}$ mM is the equilibrium intracellular Ca^{2+} concentration, $A = 2 \times 10^{-4}$ mM cm^2/(ms μA) and τ = 160 ms.

Synaptic Currents

$GABA_A$ and AMPA synaptic currents are given by

$$I_{syn} = E\ g_{syn}\ [O]\ (V - E_{syn}) \quad \text{(A5)}$$

where g_{syn} is the maximal conductance and E is a depression variable. The reversal potential is E_{AMPA} = 0 mV for AMPA receptors and E_{GABAA} = –70 mV for $GABA_A$ receptors. The fraction of open channels [O] is calculated according to the kinetic equation

$$d[O]/dt = \alpha(1 - [O])[T] - \beta[O],\ [T] = A\ \Theta(t_0 + t_{max} - t)\ \Theta(t - t_0) \quad \text{(A6)}$$

where $\Theta(x)$ is the Heaviside function, t_0 is the time instant of receptor activation. The parameters for the neurotransmitter pulse were amplitude A = 0.5 and duration t_{max} = 0.3 ms. The rate constants, α and β, were α = 10 ms and β = 0.25 ms for $GABA_A$ synapses and α = 0.94 ms and β = 0.18 ms for AMPA synapses. E was calculated according to the interactive scheme (Tsodyks and Markram, 1997):

$$E_{n+1} = 1 - [1 - E_n(1 - U_{SE})]e^{-\Delta t/\tau} \quad \text{(A7)}$$

where Δt is the time interval between nth and $(n+1)$th spike, τ = 700 ms is the time constant of recovery of the synaptic resources and U_{SE} is the fractional decrease of synaptic resources after an action potential which was varied between 0.07 and 0.15.